

Detecting Ocean Surface Winds Using TRMM Precipitation Radar

EASTWOOD IM and LI LI

*Jet Propulsion Laboratory, California Institute of Technology
4800 Oak Grove Drive, Pasadena, California 91109, USA
Tel: (1) 818-354-0492, Email: eastwood.im@jpl.nasa.gov*

ABSTRACT

Although designed specifically for the measurement of precipitation in the atmosphere, the Precipitation Radar (PR) onboard the Tropical Rainfall Measuring Mission (TRMM) satellite also measures the normalized radar cross-section at the Earth's surface. As such, this instrument provides an interesting opportunity to explore an alternative radar configuration in the satellite remote sensing of ocean winds. In particular, it can measure the strength of the ocean winds in relatively higher spatial resolution as compared to the conventional scatterometer systems presently in use. The addition of wind sensing capability to precipitation radar also complements its rain profiling capability nicely and allows coincident wind and rain measurements. In this paper, we discuss the new ocean wind algorithm developed specifically for TRMM PR using maximum likelihood estimation. A unique feature of this wind algorithm is its capability to incorporate measurement sensitivity and noise information consistently in both the along-track and cross-track directions. This PR wind algorithm has been tested using data from the TRMM Microwave Imager (TMI) and NASA QuikSCAT scatterometer. Excellent agreement on the retrieved wind strengths is achieved among three sensors.

Keywords: Ocean Surface Wind, Precipitation Radar, TRMM, Scatterometry

1. INTRODUCTION

For years, spaceborne scatterometry has been used successfully to retrieve the ocean surface wind field based on measurements of the normalized radar cross section, denoted as σ° ("sigma-zero"), at the Earth's surface level (Naderi et al, 1991). Over the ocean, the radar backscattering power depends not only the magnitude of the wind stress, but also on the wind direction relative to the radar beam. Therefore estimates of ocean surface wind vector can be obtained by acquiring radar backscattering measurements from different viewing angles. During past decades, many satellite scatterometers have been launched into space. The European Space Agency launched the first two operational scatterometers on board the European Remote Sensing Satellites (ERS-1 and ERS-2) in 1991 and 1995, respectively (Attema, 1991). Both scatterometers operate at C-band to minimize the effect of rain and atmospheric water vapor content. But they have relatively low resolution (50 km) and narrow swath (500 km). In the United States, much of the scatterometry efforts have been focused on Ku-band. In 1978, an experimental scatterometer, called Seasat Scatterometer (SASS), was launched into space on board the NASA satellite Seasat. SASS systematically collected σ° at Ku-band over a large range of incidence angle (0° to 50°). This σ° data set led to the construction of a Geophysical

Model Function (GMF), namely the SASS-2 model function (Schroeder et al., 1982; Wentz et al., 1984). Inversion techniques were also developed to retrieve the surface wind field from σ° measurements using the SASS-2 model function. In 1996, another Ku-band scatterometer, the NASA Scatterometer (NSCAT), was placed on low Earth orbits to obtain continuous surface wind measurements over the global ocean. The NSCAT used stick antennas and frequency sampling techniques to obtain 50 km resolution and two 600 km swaths coverage, separated by a gap of approximately 330 km. It acquired 16 measurements for each sample point on the sea surface to remove ambiguity in wind direction retrievals. The mission was successful in achieving its scientific goal of 2 m/s wind speed and 20° wind direction retrieval accuracies and spatial and temporal coverage before its loss after 9 months of in-orbit operations due to failure of satellite power (Graf et al., 1998; Jones et al., 1999; Liu et al., 1997). The SeaWinds scatterometer on QuikSCAT was then quickly launched into space in 1999 to replace NSCAT. The SeaWinds uses a rotating dish antenna and temporal and frequency sampling techniques to obtain 25 km resolution and a continuous 1800 km swath, which eliminates the null region inherent in the NSCAT swath (Schlax et al., 2001; Spencer et al., 2000).

Though designed specifically for the measurement of precipitation profiles in the atmosphere, the spaceborne Precipitation Radar (PR), scanning cross-track over $\pm 17^\circ$, onboard the Tropical Rainfall Measuring Mission (TRMM) satellite (Kummerow et al., 1998, 2000) also measures the normalized radar cross section of the Earth's surfaces. As such, this instrument provides an interesting opportunity to explore the benefits and pitfalls of alternative radar configurations in satellite remote sensing of ocean winds. The small incidence angles of the PR beam and the single look capability of its cross-track scan geometry may act to limit its wind retrieval potential using traditional scatterometer techniques. Nonetheless, the small horizontal footprint and vertical range gate of the PR offer other advantages over the conventional scatterometer systems presently in use. More important, the potential addition of wind sensing capability to the TRMM PR will complement its rain profiling skills in providing coincident wind and rain observations at the same high spatial resolution, which represents a significant improvement in science value over the individually generated wind and rain measurements using separated sensors at different spatial resolutions. Also interesting and equally important is the rain profiling capability of the PR at 250-m resolution, which can be readily used to detect and remove rain-contaminated surface backscattering data during the wind retrieval process. In addition, its simultaneous measurements of surface rainfall and surface backscattering can provide direct quantifications of rain contamination of the surface backscattering cross-sections. Such results will benefit the scatterometers in their ability to measure wind over the raining oceanic areas. Another important feature for the TRMM PR is its fine-resolution footprint, 4.3 km X 4.3 km. For comparison, current scatterometers can only provide 25-km resolution wind as a standard product, and 12.5-km wind as a research product.

The goal of this paper is to exploit the potential utility of cross-track scan precipitation radar as an ocean wind sensor. To this end, we derived an oceanic geophysical model function tailored toward TRMM PR by relating the PR σ° measurements with collocated wind retrievals from TRMM Microwave Imager (TMI). Based on this PR σ° model function, a field-wise wind retrieval algorithm is developed using maximum likelihood estimation. The wind field is then derived by weighting all the σ° measurements with their associated uncertainties given by the PR model function. Finally, we compare the PR derived wind fields against the TMI and QuikSCAT wind retrievals. It is worth noting that this comparison is performed over only one-month period, and it is not our objective here to develop a well-calibrated operational wind algorithm for precipitation radar.

2. GEOPHYSICAL MODEL FUNCTION FOR THE σ° OBSERVED BY TRMM PRECIPITATION RADAR

The SASS-2 Geophysical Model Function (GMF) was constructed by Wentz et al. (1984) based on statistics of σ° measurements acquired by SASS from 0° to 50° incidence angles. The validity and robustness of such a model function were also tested later with the NSCAT σ° measurements, which were acquired at incidence angles between 18° and 57° for the gain of high σ° sensitivities in wind speed and direction. In this analysis, we adopt the SASS-2 model function instead of the NSCAT model function because the SASS-2 model function is more appropriate for the near-nadir ($\pm 17^\circ$) σ° measurements obtained by TRMM PR. Nevertheless, the PR has slightly different frequency than SASS, 13.8 GHz for PR and 14.6 GHz for SASS, as well as different instrument configuration, so systematic difference between PR data and SASS model function has to be removed before the model can be applied. Taking an approach similar to those used to derive the NSCAT models, we will co-locate the PR data with the brightness temperature measurements acquired by the TRMM Microwave Imager (TMI), and then use the collocated wind speed from TMI to calibrate SASS model function toward PR data.

The geophysical model function can be written in a general form as

$$\sigma^\circ = F_p(w, \theta, \phi) \quad (1)$$

where σ° is the sea surface normalized radar backscattering coefficient; p is polarization (TRMM PR uses horizontal polarization), w is the sea surface wind speed; θ and ϕ are the incidence angle and relative wind direction, respectively. θ represents the wind direction dependence of σ° which increases with both wind speed and incidence angle. At small incidence angles (0° to 8°), the wind direction dependence is quite weak, thus, we dropped the wind direction dependence in the SASS-2 model function.

For simplicity, we assume that the bias between the SASS-2 model function and PR data is only a function of incidence angle. To assess these bias, we feed retrieved wind speed from TMI (Connor and Chang, 2000) into SASS-2 model function and compare the simulated NRCS (σ_s°) with their corresponding PR measurement (σ_m°). If we denote model errors as $\Delta\sigma^\circ$, then

$$\Delta \sigma^o(\theta) = \sigma_m^o(w, \theta) - \sigma_s^o(w, \theta) \quad (2)$$

Note that this model error contains not only errors in model function but also errors in instrument calibration, and possibly frequency difference between the TRMM PR and the SASS. The PR frequency is 13.8 GHz and SASS is at 14.6 GHz. Wind direction also is an error source but should be a random noise rather than a bias. Figure 1 plots model bias $\eta(\theta)$ and variance $\delta(\theta)$ versus incidence. In general, both $\eta(\theta)$ and $\delta(\theta)$ are symmetric about nadir. $\eta(\theta)$ exhibits a large bias around 10° , to which errors in model function and radar calibration may all contribute. On the other hand, the minimum in $\delta(\theta)$ should be mostly due to the insensitivity of σ^o to wind speed at 10° incidence angle. Although $\delta(\theta)$ cannot be reduced without an improvement in model function, $\eta(\theta)$ can be readily removed from the model function. To tailor the model function toward the PR data, we adjusted the SASS-2 model function by adding $\eta(\theta)$ to it. Hereafter we will call this adjusted SASS-2 model function the SASS-2/PR model function.

In Figure 2, PR σ^o observations are plotted against wind speed retrievals from TMI for several different PR incidence angle bins. The SASS-2/PR model function for the mean incidence angle of each corresponding angle bin is also plotted for comparison. The agreement between model function and the PR data is excellent, which indicates that σ^o measurements can be largely explained by ocean wind fields. Note that there is no bias between the new model function (SASS-2/PR) and PR data.

3. RETRIEVING OCEAN SURFACE WIND SPEED FROM TRMM PR

As a precipitation radar, TRMM PR has very high vertical resolution (~ 250 m) and small footprint (~ 4.3 km). It can easily separate rainy cells from rain-free cells due to its range gate function. But the PR only takes single-look, horizontally-polarized σ^o measurement at an incidence angle within $\pm 17^\circ$ from nadir. There is virtually no wind sensitivity around 10° incidence angle, which will create an area of absurd wind estimates if we just use point-wise wind retrieval techniques developed for scatterometers. In point-wise wind retrieval, the σ^o measurements of different sample points are not incorporated together. They are treated as if they are independent. In the real world, the σ^o measurements are indeed very noisy, but the environmental variable (ocean surface wind) that controls σ^o variation is much smoother and more coherent spatially. Therefore the wind retrieval is possible for TRMM PR if we can take advantage of this spatial coherence. Long (1989 and 1993) made use of this coherence in his field-wise retrieval

algorithm for the SASS scatterometer. He assumed that the wind speed field is relatively smooth and can be adequately described by low-order bivariate polynomials over the region of interest. We adopted his approach in our unified wind and rain algorithm.

Let us define a measurement domain by a $M \times N$ nonuniform grid with M samples in along-track and N samples in cross-track. The sample point is given by $\{x_i, y_j\}$, and $i = 1, \dots, M$; $j = 1, \dots, N$, and its corresponding measurement is $\sigma_m^o(i, j)$, incidence angle $\theta(i, j)$. For a given wind field $w(x, y)$, log likelihood function $LH(w)$ for $w(x, y)$ given all the measurements $\sigma_m^o(x_i, y_j)$, after removing all rainy cells, is then,

$$\begin{aligned} LH(w) &= \sum \sum \log p\{\sigma_m^o(x_i, y_j) | w_{ij}\} \\ &= -\frac{1}{2} \sum_{i=0}^M \sum_{j=0}^N \log \delta(\theta_{ij}) - \\ &\quad \sum \sum \frac{\{\sigma_m^o(x_i, y_j) - \sigma_s^o(w_{ij}, \theta_{ij})\}^2}{2\delta(\theta_{ij})} R_{ij} \end{aligned}$$

where R_{ij} is a flag used to remove rainy cells detected by the radar. Specifically, $R_{ij} = 0$ for rainy cells and $R_{ij} = 1$ for rain-free cells. The wind field over the region of interests can be estimated with the maximum Likelihood estimation.

4. RESULTS AND DISCUSSION

To quantify the performance of our PR wind algorithm, we compare the wind retrieved from TRMM PR and TMI over rain-free ocean. Figure 3a is a scatter plot of TMI winds versus the PR spatially averaged winds for the month of August 1998. The 45°-line represents perfect agreement. Only rain-free scenario is included in the plot. The total number of wind comparisons is 30840. In general, there is an excellent agreement between TMI and PR retrieved winds. Their correlation coefficient is 0.72 with a mean TMI minus PR difference of -0.14 m/s and a standard deviation of 1.7 m/s. To examine the wind difference as a function of the wind speed, the wind speed pairs in Figure 3a are first stratified into 1 m/s TMI wind speed bins; then, the variation of the PR wind is calculated for each bin in term of its mean (bias) and standard deviation, which are plotted in Figure 3b against the mean wind speed of TMI. The vertical error bar is one standard deviation in each bin. From 5 to 16 m/s, the mean wind difference between PR and TMI is quite small, mostly below 0.4 m/s. For winds below 5 m/s, the mean PR winds are consistently larger than those of TMI, as much as 2.2

m/s. The standard deviation of the PR minus TMI wind speed difference, as indicated by the error bar, increases steadily with TMI average wind speed. We also examined the TMI and PR wind difference as a function of PR incidence angle. We found that their mean difference is always very small, mostly below 0.2 m/s, and their standard deviation is quite constant around 1.7 m/s.

QuikSCAT wind is another rigorously validated wind products. To further evaluate our TRMM PR wind algorithm, we compare TRMM PR and QuikSCAT wind speed data by collocating these two sensors in space and time, then averaging the PR data to the QuikSCAT spatial resolution. The comparison was done for the period of 15 August -- 14 September 2000, from which 1499 wind speed match-ups were collected. They were compared on Figure 4 in a similar way as in Figure 3. In general, the agreement between the PR and QuikSCAT is excellent except at low and high winds. The correlation between QuikSCAT and PR average wind speed is very high with a correlation coefficient of 0.94. Note that the QuikSCAT and PR data are completely independent of each other, and yet the QuikSCAT minus PR average wind difference is only 0.656 m/s with a standard deviation of 1.11 m/s.

Finally, we performed χ^2 tests to see if the distance between simulated and measured σ^o is within the model uncertainties. This distance can be quantitatively measured by the goodness-of-fit parameter, which is approximately equal to one for a moderately good fit; the smaller the goodness-of-fit parameter, the better the fit. Our test shows that most goodness-of-fit values are between 0.2 and 0.8. Therefore our model function fits the PR σ^o observations quite well, suggesting that that our PR wind algorithm is indeed sufficiently accurate to model the PR measurements.

5. SUMMARY

An algorithm is developed to retrieve ocean surface wind speed from surface backscattering measurements by TRMM PR. Applications of this algorithm show excellent agreement with wind fields retrieved from TRMM TMI and QuikSCAT data, suggesting that TRMM PR σ^o measurements could be used to infer ocean surface wind speed with accuracy comparable to those of TRMM TMI and QuikSCAT, which are generally less than 2 m/s.

ACKNOWLEDGEMENTS

The authors wish to acknowledge helpful discussion with Drs. R. D. West and R. S. Dunbar. Dr. Dunbar also kindly provided SASS-2 and NSCAT2 model

functions to us. Dr. Connor of NOAA/NESDIS provided his TRMM/TMI ocean surface wind retrieval algorithm. This research was performed at the Jet Propulsion Laboratory, California Institute of Technology for the TRMM Mission, under contract with the National Aeronautics and Space Administration.

REFERENCES

- Attema, E., 1991: The active microwave instrument on-board the ERS-1 satellite. *Proceedings IEEE*, **79**, 791-799.
- Connor, L. and P. Chang, 2000: Ocean surface wind retrievals using the TRMM Microwave Imager. *IEEE Trans. Geosci. Remote Sensing*, **38**, 2009-2016.
- Graf, J., C. Sasaki, C. Winn, W.T. Liu, W. Tsai, M.H. Freilich, and D. Long, 1998: NASA scatterometer experiment, *Asta Astronautica*, **43**, 397-407.
- Jones, W. L., V. J. Cardone, W. J. Pierson, J. Zec, L. P. Rice, A. Cox, and W. B. Sylvester, 1999: NSCAT high-resolution surface wind measurements in typhoon Violet. *J. Geophys. Res.*, **104**, 11,247-11,259.
- Kim, Y. J., K. S. Pak, C. S. Hsu, P. S. Callahan, R. S. Dunbar, S. V. Hsiao, and A. Zhang, 1998: Improving the sea surface wind retrieval algorithm for NASA Scatterometers using atmospheric boundary layer models. *Proc. IGARSS '98*, 1115-1117.
- Kummerow, C., W. Barnes, T. Kouz, J. Shiue, and J. Simpson, 1998: The Tropical Rainfall Measuring Mission (TRMM) sensor package. *J. Atmos. Oceanic Tech.*, **15**, 809-817.
- Kummerow, C., J. Simpson, O. Thiele, W. Barnes, A.T.C. Chang, E. Stocker, R.F. Adler, A. Hou, R. Kakar, E. Wentz, P. Ashcroft, T. Kouz, Y. Hong, K. Okamoto, T. Iguchi, H. Kuroiwa, E. Im, Z. Haddad, G. Huffman, B. Ferrier, W.S. Olson, E. Zipser, E.A. Smith, T.T. Wilheit, G. North, T. Krishnamurti, and K. Nakamura, 2000: The status of the Tropical Rainfall Measuring Mission (TRMM) after 2 years in orbit. *J. Appl. Meteor.*, **39**, 1965-1982.
- Liu, W.T., W. Tang, and R.S. Dunbar, 1997: Scatterometer observations extratropical transition of Pacific typhoons, *EOS Transactions, American Geophysical Union*, **78**, 237, 240.
- Long, D., 1989: Model-based estimation of wind fields over the oceans from wind scatterometer measurements. Ph.D. dissertation, University of Southern California.
- Long, D. 1993: Wind field model-based estimation of Seasat scatterometer winds. *J. Geophys. Res.*, **98**, 14,651-14,669.
- Naderi, F.M., M.H. Freilich, and D. Long, 1991: Spaceborne radar measurements of wind velocity over the ocean – An overview of the NSCAT scatterometer system, *Proc. IEEE*, **79**, 850-866.
- Schlag, M.G., D.B. Chelton, and M.H. Freilich, 2001: Sampling errors in wind fields constructed from single and

tandem scatterometer datasets, *J. Atmos. Oceanic Tech.*, **18**, 1014-1036.

Schroeder, L. C., D. H. Boggs, G. Dome, I. M. Halberstam, W. L. Jones, W. J. Pierson, and F. J. Wentz, 1982: The relationship between wind vector and normalized radar cross section used to derive Seasat-A satellite scatterometer winds. *J. Geophys. Res.*, **87**, 3318-3336.

Spencer, M.W., C.L. Wu, and D.G. Long, 2000: Improved resolution backscatter measurements with the SeaWinds pencil-beam scatterometer, *IEEE Trans. Geosci. Remote Sensing*, **38**, 89 - 104.

Wentz, F., S. Peteherych, and L. A. Thomas, 1984: A model function for ocean radar cross section at 14.6 GHz. *J. Geophys. Res.*, **89**, 3689-3704.

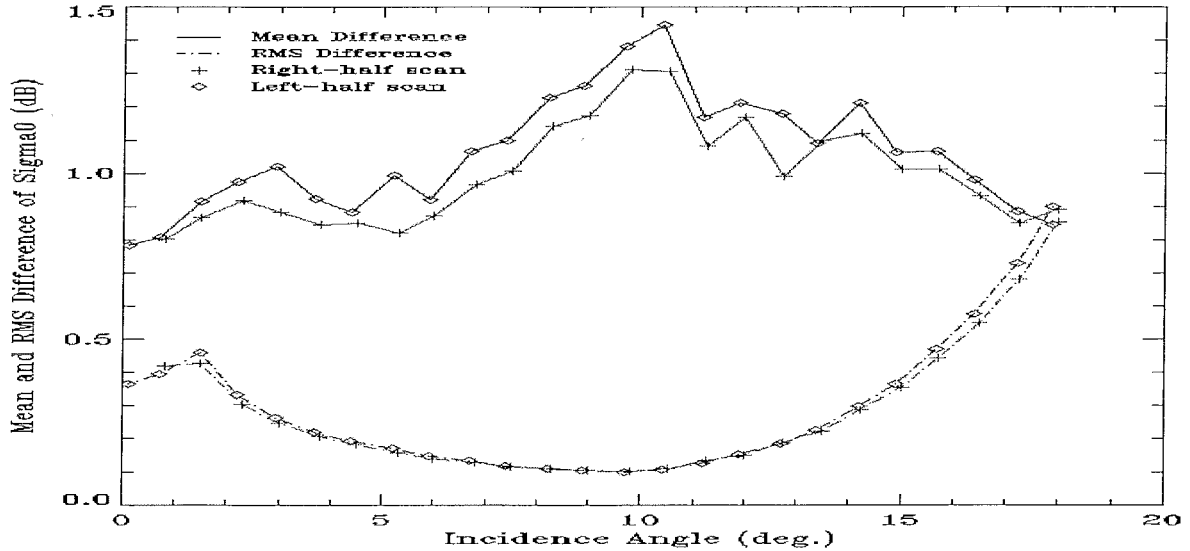


Figure 1. The differences between simulated and observed σ^0 of PR versus incidence angle bins. The data cover three months from August to October, 1998.

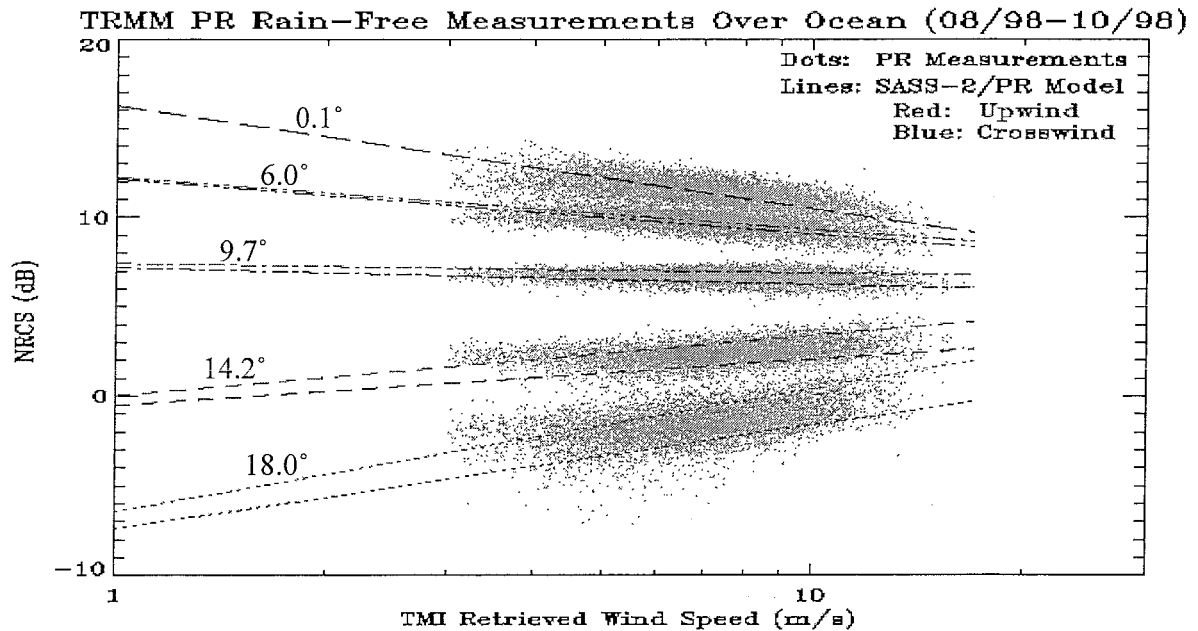


Figure 2. PR σ^0 observations versus retrieved TMI wind speeds for five different PR incidence angle bins. The SASS-2/PR model function is also plotted for comparison.

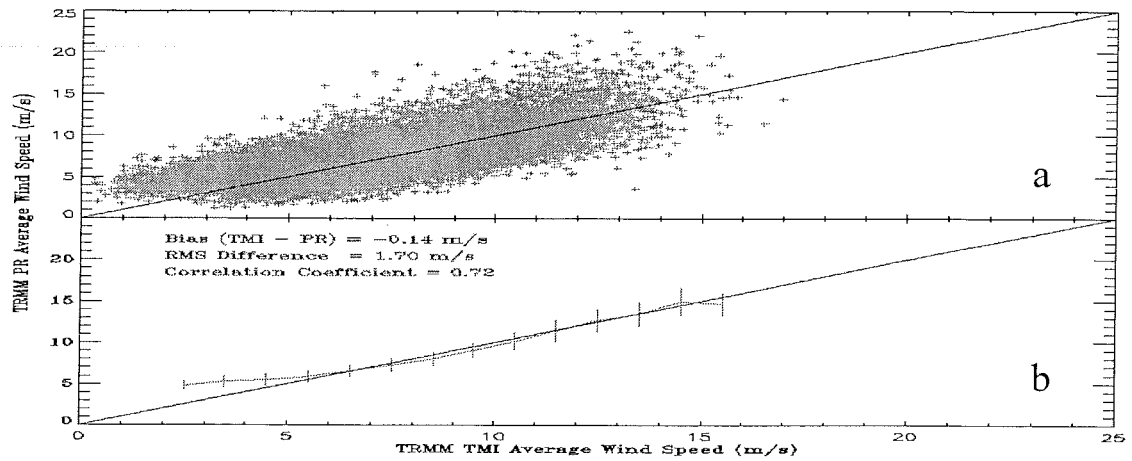


Figure 3. Comparison of the ocean surface winds retrieved from the TRMM PR and TMI. The data cover all the coincident PR and TMI rain-free measurements of for August 1998.

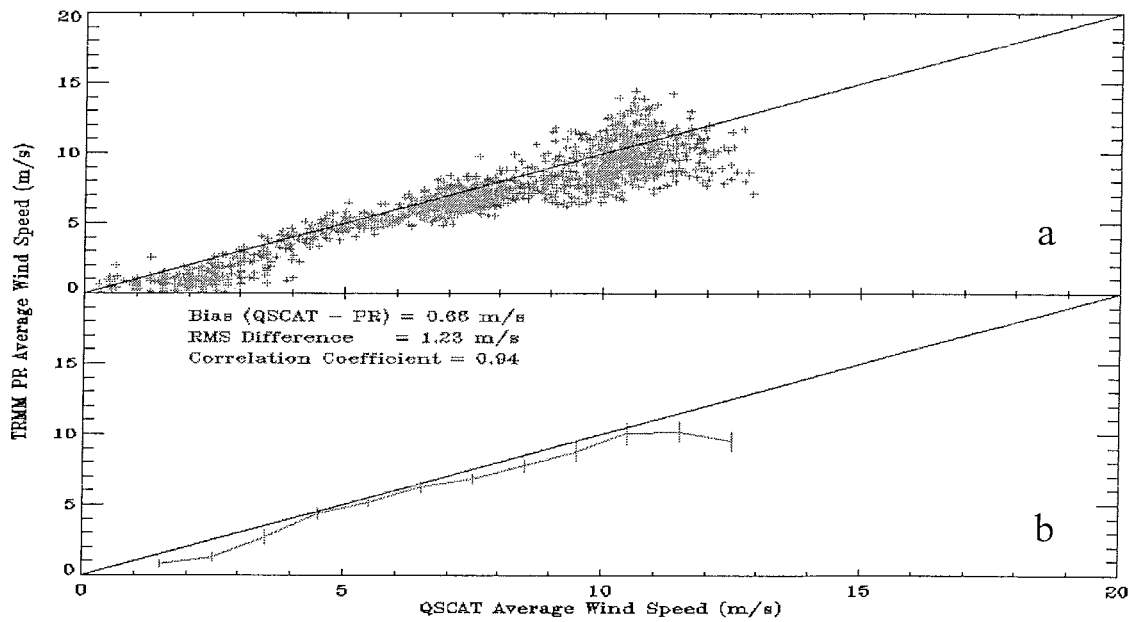


Figure 4. Comparison of the ocean surface winds retrieved from the TRMM PR and QuikSCAT. The data cover all the coincident PR and QuikSCAT rain-free measurements of for 15 August - 14 September 2000.